Geophysical Research Letters

RESEARCH LETTER
10.1029/2023GL104417

# Quantifying the Efficiency of Stratospheric Aerosol Geoengineering at Different Altitudes

**Walker R. Lee[1], Daniele Visioni[1,2], Ewa M. Bednarz[1,3,4], Douglas G. MacMartin[1], Ben Kravitz[5,6], and Simone Tilmes[2]**

[1]Sibley School of Mechanical and Aerospace Engineering, Cornell University, Ithaca, NY, USA, [2]Atmospheric Chemistry, Observations, and Modeling Lab, National Center for Atmospheric Research, Boulder, CO, USA, [3]Cooperative Institute for Research in Environmental Sciences (CIRES), University of Colorado Boulder, Boulder, CO, USA, [4]NOAA Chemical Sciences Laboratory (NOAA CSL), Boulder, CO, USA, [5]Department of Earth and Atmospheric Sciences, Indiana University, Bloomington, IN, USA, [6]Atmospheric Sciences and Global Change Division, Pacific Northwest National Laboratory, Richland, WA, USA

**Abstract** Stratospheric aerosol injection (SAI) of reflective sulfate aerosols has been proposed to temporarily reduce the impacts of global warming. In this study, we compare two SAI simulations which inject at different altitudes to provide the same amount of cooling, finding that lower-altitude SAI requires 64% more injection. SAI at higher altitudes cools the surface more efficiently per unit injection than lower-altitude SAI through two primary mechanisms: the longer lifetimes of $SO_2$ and $SO_4$ at higher altitudes, and the water vapor feedback, in which lower-altitude SAI causes more heating in the tropical cold point tropopause region, thereby increasing water vapor transport into the stratosphere and trapping more terrestrial infrared radiation that offsets some of the direct aerosol-induced cooling. We isolate these individual mechanisms and find that the contribution of lifetime effects to differences in cooling efficiency is approximately five to six times larger than the contribution of the water vapor feedback.

**Plain Language Summary** Stratospheric aerosol injection (SAI)—the artificial introduction of reflective droplets, called aerosols, into the middle atmosphere–could reflect a small portion of sunlight and cool the planet in order to temporarily reduce the impacts from global warming. Injecting the aerosols at higher altitudes would be more expensive, but it would also be more efficient because the aerosols would last longer before falling out of the atmosphere. Additionally, injecting at a lower altitude would cause more water vapor to enter the middle atmosphere; since water vapor is a greenhouse gas, this would increase the greenhouse effect, meaning more aerosols would be needed to cool the surface to a desired temperature. In this study, we directly compare high-altitude SAI to low-altitude SAI to determine how much more efficient it is to inject at a higher altitude, and we break down the different factors that effect efficiency to see which has the biggest effect.

**Key Points:**

- We compare two stratospheric aerosol injection strategies which inject $SO_2$ at different altitudes to meet the same temperature target
- The low altitude strategy requires two thirds more injection to provide the same amount of cooling
- We isolate and quantify the different factors which cause the high altitude injection strategy to cool the surface more efficiently

**Supporting Information:**

Supporting Information may be found in the online version of this article.

**Correspondence to:**

W. R. Lee,
wl644@cornell.edu

**Citation:**

Lee, W. R., Visioni, D., Bednarz, E. M., MacMartin, D. G., Kravitz, B., & Tilmes, S. (2023). Quantifying the efficiency of stratospheric aerosol geoengineering at different altitudes. *Geophysical Research Letters*, *50*, e2023GL104417. https://doi.org/10.1029/2023GL104417

Received 3 MAY 2023
Accepted 12 JUL 2023

**Author Contributions:**

**Investigation:** Walker R. Lee, Daniele Visioni, Ewa M. Bednarz
**Methodology:** Simone Tilmes
**Supervision:** Douglas G. MacMartin
**Writing – original draft:** Walker R. Lee
**Writing – review & editing:** Daniele Visioni, Ewa M. Bednarz, Douglas G. MacMartin, Ben Kravitz, Simone Tilmes



## 1. Introduction

Stratospheric aerosol injection (SAI) is a proposed method of climate intervention in which aerosols are introduced into the stratosphere to reflect sunlight. Alongside emissions cuts and carbon dioxide removal, SAI could cool the surface and mitigate or prevent some impacts of global warming. In 2021, the National Academies recommended that a research agenda be established to investigate the efficacy, feasibility, and risks of SAI and other methods of solar geoengineering, with the ultimate purpose of informing future decision making (National Academies of Sciences, Engineering, and Medicine, 2021). The effects of SAI on the surface climate and atmospheric circulation would depend on the quantity, latitude, seasonality, and altitude of $SO_2$ injection (Bednarz, Butler, et al., 2023; Bednarz, Visioni, et al., 2023; Visioni et al., 2023; Zhang et al., 2023). The choice of injection altitude can affect the impacts of SAI through various mechanisms (Tilmes, Richter, Mills, et al., 2018), which we divide into two broad categories:

- Lifetime and size effects, which affect aerosol optical depth (AOD) produced per unit $SO_2$ injection: a higher injection altitude places aerosols deeper into the upper branch of the Brewer-Dobson circulation (BDC), resulting in longer aerosol lifetime against sedimentation (Niemeier et al., 2011) and thus more forcing per unit injection. $SO_2$ injected at lower altitudes can also leave the stratosphere before oxidizing; we do not distinguish between these processes. Niemeier et al. (2011), Aquila et al. (2014), and Tilmes et al. (2017) all report higher simulated aerosol burdens in the upper stratosphere for higher-altitude injection than for lower-altitude

injection. However, longer aerosol lifetime also results in aerosol growth due to coagulation; aerosols larger than the optimal effective radius to reflect sunlight (Dykema et al., 2016) cool less efficiently and also deposit faster, which acts to offset the effects of longer sulfur lifetime. Different studies report different findings on the relative magnitudes of the lifetime and coagulation effects: Using the Community Earth System Model (CESM1), Tilmes et al. (2017) reported a smaller AOD per unit sulfate burden for higher-altitude SAI, but higher-altitude SAI still achieved a higher AOD per unit injection, indicating the larger aerosol size did not fully negate the increased AOD of the longer lifetime. However, in a different model (LMDZ-S3A), Kleinschmitt et al. (2018) found that particle growth was sufficient to cancel out the benefit of a higher sulfur lifetime, and that same-quantity injections at different altitudes produced comparable radiative forcing. The relative importance of these processes may also depend on the latitude of injection; Kleinschmitt et al. injected at the equator, while Tilmes et al. (2017) considered injections at several latitudes. The latter reported that the incremental increase with altitude of AOD per unit injection is smallest at the equator and increases as injection location moves further from the equator; this is because, as mentioned above, placing aerosols into a lower-altitude branch of the BDC causes them to be removed from the stratosphere more quickly, and this effect is stronger at higher latitudes. Finally, a lower-altitude aerosol layer can also see increased aerosol size due to hygroscopic growth (K. Krishnamohan et al., 2020) as lower-stratospheric heating increases water vapor transport into the lower stratosphere (see radiative feedbacks below), which could increase or decrease AOD per unit $SO_2$ injection depending on the resultant aerosol size.

- Radiative feedbacks, which affect the amount of surface cooling produced per unit of AOD. First, a sulfate aerosol layer closer to the tropopause heats the tropical tropopause layer, allowing more water vapor to transport into the stratosphere. The increase in lower stratospheric water vapor results in a net increase of trapped terrestrial infrared radiation, requiring additional $SO_2$ injection to compensate and decreasing the efficacy of SAI as a whole (Bednarz, Butler, et al., 2023; Bednarz, Visioni, et al., 2023; Heckendorn et al., 2009; K.-P. S.-P. Krishnamohan et al., 2019; Visioni et al., 2017; Quaglia et al., 2022). Second, a decrease in the vertical temperature gradient in the upper troposphere can result in a thinning of high cirrus clouds which trap outgoing terrestrial radiation, increasing the overall cooling effect of SAI (Visioni et al., 2018). Lastly, the reduction in solar radiation reaching the troposphere under SAI could also reduce OH concentrations and thus increase methane lifetime, strengthening the greenhouse effect further (Visioni et al., 2017). However, this effect is not present in CESM1 because stratospheric aerosols are not coupled to the photolysis scheme.

In this study, we directly compare higher-altitude and lower-altitude injection using an Earth system model to examine how efficiently they can meet the same surface temperature target (i.e., how much $SO_2$ is required to provide a certain amount of cooling), and we isolate and quantify the relative contributions of lifetime and size effects and radiative feedbacks in these simulations.

## 2. Climate Model and Simulations

The simulations considered in this study use Version 1 of the fully-coupled Community Earth System Model (CESM1), with the Whole Atmosphere Community Climate Model (WACCM) as the atmospheric component (Hurrell et al., 2013). The model is run at a horizontal resolution of 0.9° latitude by 1.25° longitude with 70 vertical layers reaching up to approximately 140 km ($10^{-6}$ hPa). Aerosols are simulated using the Modal Aerosol Module (MAM3), which is coupled to chemistry and radiation and describes the aerosol distribution using three modes: Aitken, accumulation, and coarse (Liu et al., 2012; Mills et al., 2017).

This study considers three sets of simulations: RCP8.5, iHIGH, and iLOW. RCP8.5 is a high-emissions global warming scenario (Meinshausen et al., 2011), and the iHIGH and iLOW SAI strategies, which both branch from RCP8.5, simulate "high-altitude" (23–25 km) and "low-altitude" (19–20 km) SAI, respectively, to offset the warming from RCP8.5. RCP8.5 begins in 2015, the SAI simulations branch from RCP8.5 in 2020, and all three simulations run until 2100. iHIGH is described by Tilmes, Richter, Kravitz, et al. (2018) as the Geoengineering Large Ensemble (GLENS), using the four-latitude injection approach described by Kravitz et al. (2017), and iLOW is described by Tilmes et al. (2021) as the "Low" experiment. Both iHIGH and iLOW simulate $SO_2$ injection into the stratosphere at 30°N, 15°N, 15°S, and 30°S to maintain the global mean temperature at the 2010–2030 RCP8.5 average while also preserving the 2010–2030 interhemispheric and equator-to-pole temperature gradients. The amount of $SO_2$ needed each year at each of the four injection latitudes to meet these targets is computed by a feedback algorithm (MacMartin et al., 2017). iHIGH injects approximately 7 km above the mean

tropopause (25 km for 15°N/S and 23 km for 30°N/S), and iLOW injects approximately 2 km above the mean tropopause (20 km for 15°N/S and 19 km for 30°N/S). iHIGH has 20 ensemble members, iLOW has 3 ensemble members, and RCP8.5 has 20 ensemble members for the 2010–2030 period and 3 for the 2030–2098 period.

## 3. Results

### 3.1. Injection Rate, Surface Response, and Stratospheric Response

Figure 1 presents $SO_2$ injection rates for iHIGH and iLOW as determined by the feedback algorithm, and changes to surface temperature. The RCP8.5 ensemble has an average temperature of 15.08°C during the 2010–2029 period (henceforth "reference period"), increasing by approximately 3.7°C by the 2070–2089 period (henceforth "experimental period"). iHIGH and iLOW aim to offset this warming; both iHIGH and iLOW match the RCP8.5 reference period temperature during the experimental period to within 0.1°C. iLOW requires approximately 64% more total injection than iHIGH to meet this goal (1a), with 38.2 Tg/yr of $SO_2$ for iHIGH and 62.6 Tg/yr for iLOW during the experimental period. The distributions of $SO_2$ injection across the four injection latitudes in the two SAI experiments are similar (1b-c), with most of the injection occurring at 30°N and 30°S and the injection at 15°S decreasing to zero as the algorithm converges (i.e., as the feedback algorithm adjusts injection rates over time to drive surface temperature toward the target state). Both strategies inject about 45% of the total injection to 30°N by the end of the century; the remainder is split between 30°S and 15°N. iLOW injects a little more to the southern hemisphere (about 40% compared to 35% in iHIGH). The patterns of surface cooling produced by the two strategies are similar (Figures 1e–1g); the differences in the Northern Hemisphere mid-to high latitudes are likely due to a stronger polar vortex response in iLOW, which merits further investigation. Changes to precipitation are also similar between the two simulations (see Figure S1 in Supporting Information S1).

### 3.2. Lifetime and Size Effects

Figure 2 plots stratospheric sulfate burden and AOD produced per unit $SO_2$ injection. Despite higher total injection rates in iLOW, iHIGH has higher concentrations of $SO_4$ spread over a larger region (2a-b). This is due to differences in sulfur lifetime; sulfur lifetime is approximately 56% longer for iHIGH than for iLOW (2c). The longer lifetime and resultant higher sulfur concentrations for iHIGH allow for more aerosol growth due to coagulation (Pierce et al. (2010); Niemeier and Timmreck (2015) - see Figure S2 in Supporting Information S1 for plots of aerosol size), and the larger particles reflect slightly less efficiently. This slightly reduces AOD per unit injection, which is about 51% higher for iHIGH relative to iLOW (Figure 2d; see Table S1 in Supporting Information S1 for calculations). However, this is only slightly smaller than the ratio of lifetimes, indicating that differences in AOD per unit injection are mainly due to differences in lifetime, and radiative changes from differences in aerosol size are a second-order effect.

### 3.3. Radiative Feedbacks

Figure 3 shows the vertical profiles of temperature for iHIGH and iLOW, as well changes to the tropopause. Both SAI strategies heat the lower stratosphere; the strongest heating is near the $SO_2$ injection sites, with iLOW showing more concentrated heating than iHIGH. This lower stratospheric heating, alongside the reduction in upper tropospheric temperatures, pushes the tropopause downward. iLOW, which has stronger heating closer to the bottom of the stratosphere, causes a larger shift in tropopause height. SAI-induced changes in tropical upper troposphere temperatures are similar for iLOW and iHIGH, indicating that changes to high cirrus clouds and their radiative impacts will be similar (Visioni et al., 2018); changes to upper troposphere cloud ice content are included in the Supporting Information S1 (Figure S3).

In Figure 4, we present the relationships between injection rate, global mean AOD, and changes to stratospheric water vapor content (relative to the reference period; the negative anomalies in Panel 4a represent changes in tropopause pressure in the first 10 years of SAI while injection rate is still small) for iHIGH and iLOW, and how these differences affect the longwave and shortwave forcing. Under comparable injection rates, iLOW results in approximately 10%–20% more stratospheric water vapor than iHIGH (Figure 4a) as the stratospheric warming occurs closer to the tropical tropopause layer. Examining the top-of-atmosphere radiation budget (Figure 4b), both strategies produce approximately 1 $W/m^2$ of net cooling, consistent with the similarity between the associated

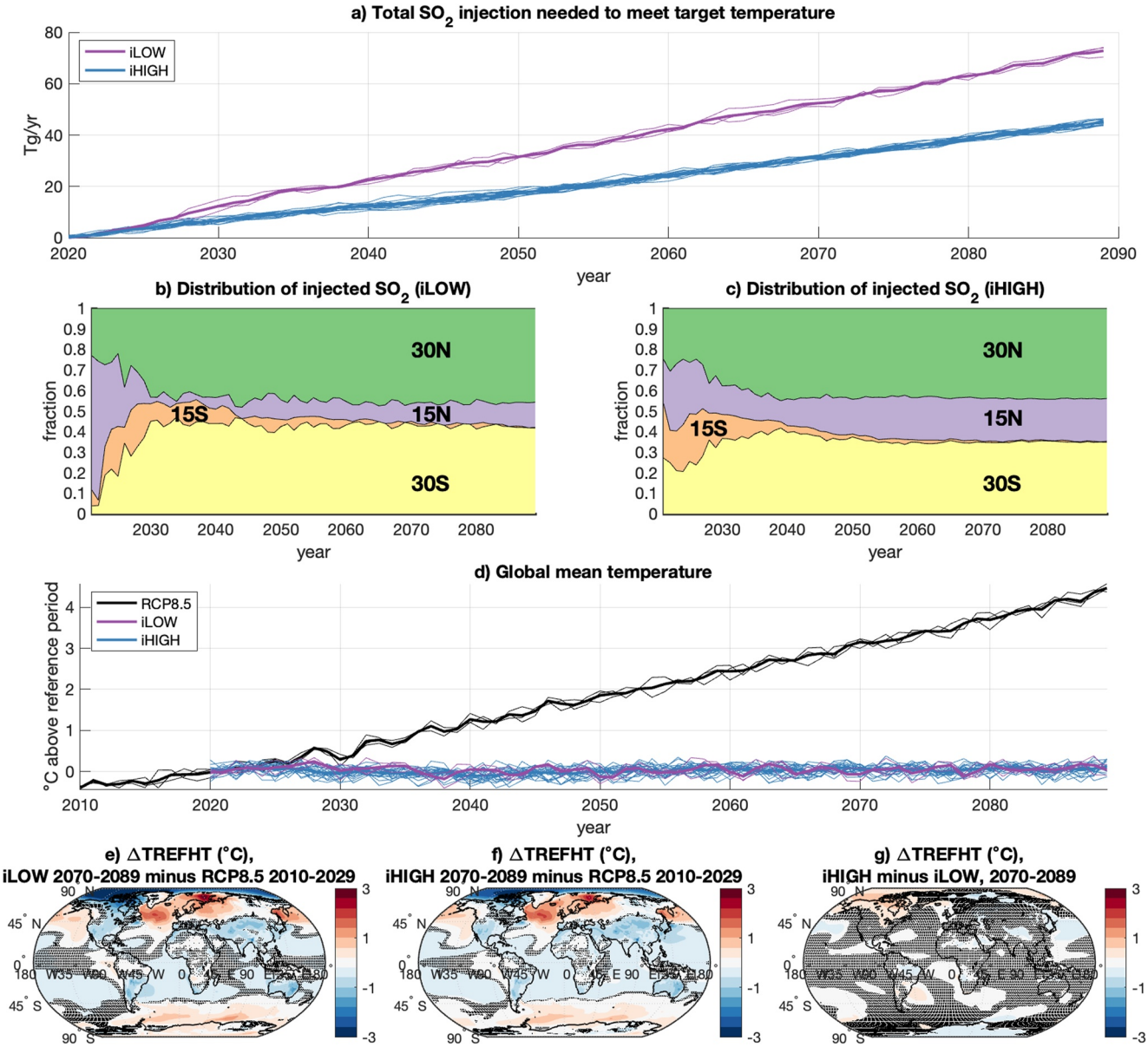


**Figure 1.** $SO_2$ injection rates and surface temperature. Panel (a) plots the total injection rates necessary in each year to maintain the desired temperature goals; faint lines denote individual ensemble members, while thick lines denote ensemble averages. Panels (b and c) plot how the total quantity injected each year is distributed across the four injection latitudes (30°N, 15°N, 15°S, and 30°S) for iLOW and iHIGH ensemble averages, respectively. Panel (d) plots annually-averaged, global mean surface temperature for iHIGH, iLOW, and RCP8.5; thick lines denote ensemble averages, while thin lines denote individual ensemble members. Panels (e and g) plot differences in surface temperature for iHIGH (2070–2089), iLOW (2070–2089), and the reference period (RCP8.5, 2010–2030); panel e plots iLOW minus the reference period, panel (f) plots iHIGH minus the reference period, and panel g plots iHIGH minus iLOW. Shading denotes regions with no significant difference according to the two-sample *t*-test at the 95% confidence level.

global mean surface temperature changes (Figure 1). However, iLOW has about 10% more trapped LW, primarily as the result of stronger stratospheric moistening, and must compensate with additional $SO_2$ injection to increase the reduction in SW by about 10%. This feedback can also be seen in the associated AOD changes (Figure 4c), which average about 10% higher globally for iLOW than for iHIGH. See Figure S4 in Supporting Information S1 for changes to radiative forcing are broken down into total, aerosol, and cloud forcing (in particular, we note that differences in cloud forcing between iLOW and iHIGH are the same order of magnitude (10%) as changes to aerosol and total forcing, indicating that differences in cloud forcing can be ruled out as a significant contributor to differences in cooling per AOD between iLOW and iHIGH).

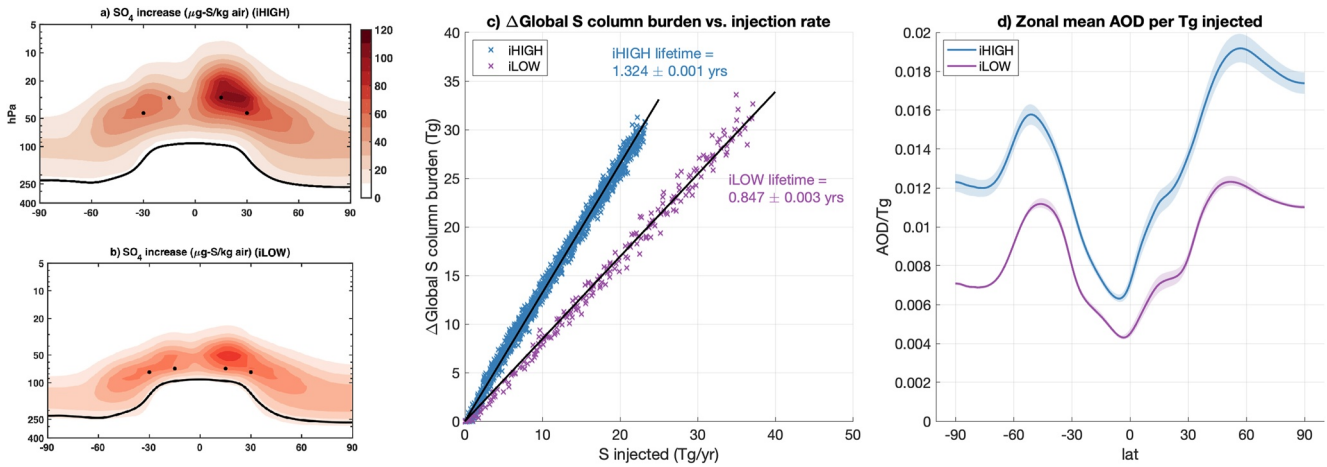


**Figure 2.** Sulfate burden and aerosol optical depth (AOD) per unit injection. Panels (a and b) plot changes to atmospheric $SO_4$ mixing ratio for iHIGH and iLOW (2070–2089), respectively, relative to the reference period (RCP8.5, 2010–2030). Black dots denote injection locations; the solid black line denotes the location of the tropopause in that simulation. Panel (c) plots changes to globally integrated sulfur column burden (iHIGH and iLOW 2070–2089 minus RCP8.5 2070–2089) as a function of injected sulfur; each point is 1 year of data. Black lines denote lines of best fit constrained through the origin; the slope of the line denotes sulfur lifetime in years, displayed as text next to each line. Panel (d) plots zonal mean day-night stratospheric 550 nm AOD divided by $SO_2$ injection rate for iHIGH and iLOW (2070–2089); shading denotes ensemble spread.

### 3.4. Quantifying the Relative Contribution of Different Factors

To determine the relative importance of lifetime and size effects and the water vapor feedback, we decompose the relationship between injection rate and surface cooling as follows:

$$\text{Cooling} = \text{injection rate} \times \frac{\text{AOD}}{\text{injection rate}} \times \frac{\text{cooling}}{\text{AOD}} \tag{1}$$

Evaluating Equation 1 for each iHIGH and iLOW, and taking the ratio:

$$\frac{\text{Cooling (iHIGH)}}{\text{Cooling (iLOW)}} = \frac{\text{inj. rate (iHIGH)}}{\text{inj. rate (iLOW)}} \times \frac{\text{AOD per inj. (iHIGH)}}{\text{AOD per inj. (iLOW)}} \times \frac{^\circ\text{C per AOD (iHIGH)}}{^\circ\text{C per AOD (iLOW)}} \tag{2}$$

Since iHIGH and iLOW provide nearly identical global mean cooling, the left side of Equation 2 is unity, and we move the ratio of injection rates to the left side:

$$\frac{\text{inj. rate (iLOW)}}{\text{inj. rate (iHIGH)}} = \frac{\text{AOD per inj. (iHIGH)}}{\text{AOD per inj. (iLOW)}} \times \frac{^\circ\text{C per AOD (iHIGH)}}{^\circ\text{C per AOD (iLOW)}} \tag{3}$$

Neglecting differences in the spatial patterns of AOD, which are small, differences in the ratios of AOD per injection rate for iLOW and iHIGH are determined by the net sum of lifetime and size effects (Figure 5a), and the differences in cooling per unit AOD are determined by radiative feedbacks (Figure 5b). Since the methane lifetime feedback is not simulated in CESM1, and differences in temperature gradients and cloud ice in the tropical upper troposphere are small between iHIGH and iLOW, the differences seen in Figure 5b are dominated by the water vapor feedback. During the experimental period, the ratio of AOD to $SO_2$ injection (lifetime and size factors) is approximately 51% higher for iHIGH compared to iLOW, and the ratio of cooling per unit AOD (the water vapor feedback) is approximately 9% higher. Therefore, Equation 3 simplifies to $1.64 \approx 1.51 \times 1.09$ (the two sides are not perfectly equal due to rounding; more detailed calculations can be found in Table S1 in Supporting Information S1), and the net contribution of lifetime and size factors (51% higher for iHIGH) is approximately 5–6 times higher than the contribution of the water vapor feedback (9% higher for iHIGH) to the increased injection rate for iLOW. This ratio is not perfectly uniform over time (Figure 5c); most prominently, AOD per unit $SO_2$ injection decreases over time for iHIGH (Figure 5a), which we attribute primarily to aerosol coagulation.

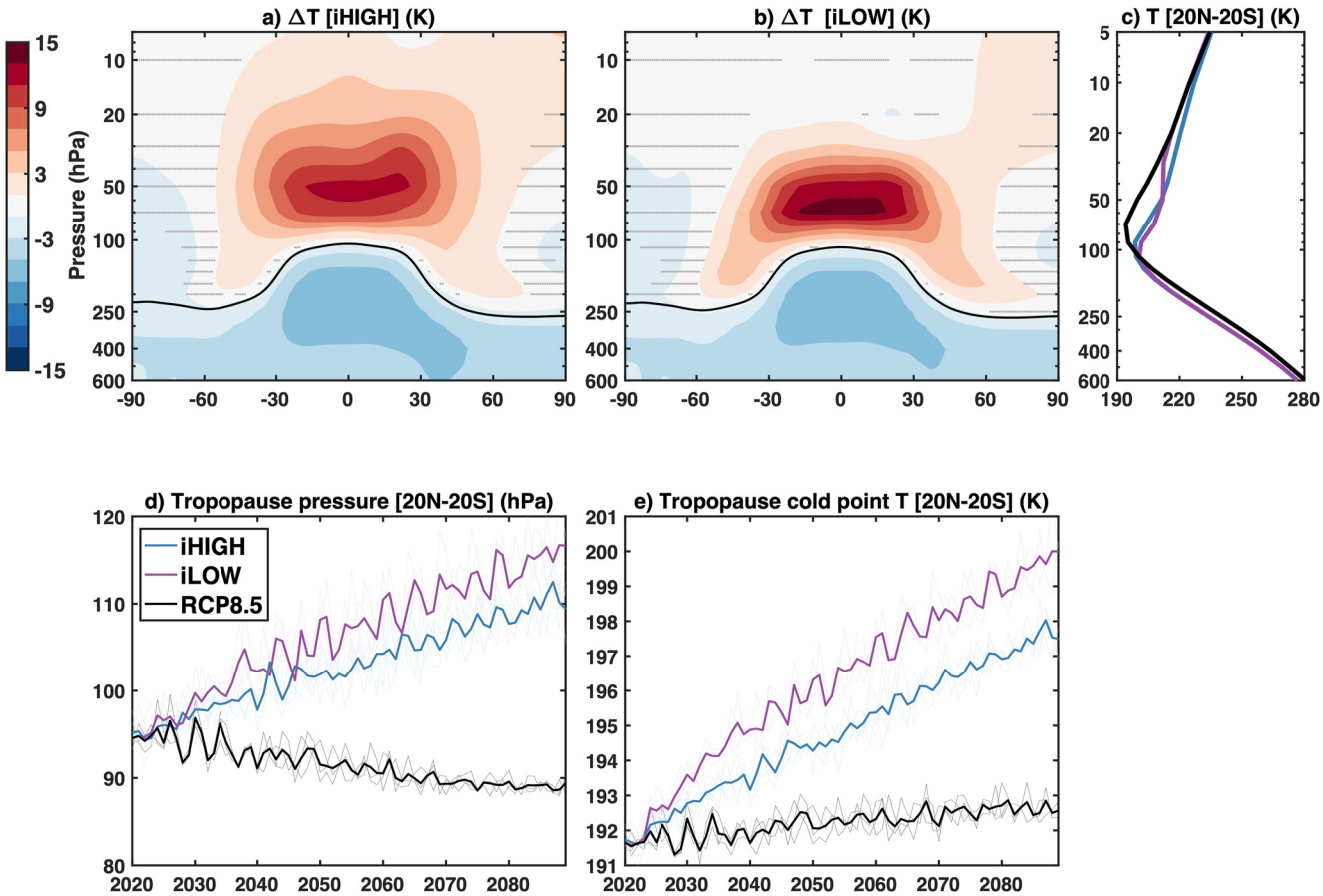


**Figure 3.** Air temperature and the tropopause. Panels (a and b) plot differences in zonally-averaged air temperature for iHIGH and iLOW (2070–2089), respectively, relative to the reference period (RCP8.5 2010–2030). Shading indicates regions with no significant difference according to the two-sample *t*-test at the 95% confidence level; the solid black line denotes the ensemble mean tropopause. Panel (c) plots average, area-weighted air temperature between 20°N and 20°S as a function of altitude for iHIGH and iLOW (2070–2089) and the RCP8.5 reference period (2010–2030). Panels (d and e) plot tropopause pressure altitude and cold-point temperature, respectively (area-weighted between 20°N and 20°S) over time for the ensemble averages of iHIGH, iLOW, and RCP8.5; faint lines denote individual ensemble members, and thick lines denote ensemble averages.

## 4. Discussion

Fully understanding possible trade-offs of using different injection altitudes, and the physical mechanisms which govern them, is necessary to inform future decision-making for SAI, as the high altitude required for tropical injection represents a significant practical barrier to implementation. Many Earth System Model simulations of SAI have assumed injection altitudes on the order of a few kilometers above the tropopause, ranging from 21 to 25 km for injection at 15°N/S and 21–23 km for injection at 30°N/S (Kravitz et al., 2017; Lee et al., 2020; MacMartin et al., 2022; Richter et al., 2022; Tilmes, Richter, Kravitz, et al., 2018; Visioni et al., 2019, 2021), but injection altitudes could range from just above the tropopause (e.g., injection altitudes of 18–19 km in the tropics) to 25 km or higher. The estimated cost of deployment increases rapidly with injection altitude (McClellan et al., 2012; Smith et al., 2022); existing commercial and military aircraft are not capable of lofting payloads of the required size to even 15 km altitude (Smith & Wagner, 2018), a deployment at 20 km would require the development of a novel aircraft (Bingaman et al., 2020), and injections at or above 25 km would likely have substantially increased cost, complexity, and risk relative to lower-altitude injections (Smith et al., 2022). While injecting less $SO_2$ overall could decrease the risk of hazards to humans and ecosystems, the increasing cost per unit injection of deployment with altitude is likely nonlinear and contains discontinuities (as any given technology will have a maximum operating altitude, deployment above which would require developing a different technology). This study considered only two sets of injection altitudes, meaning that more work is needed to fully map trade-offs (both climatological and logistical) between injections at different altitudes. For example, iLOW

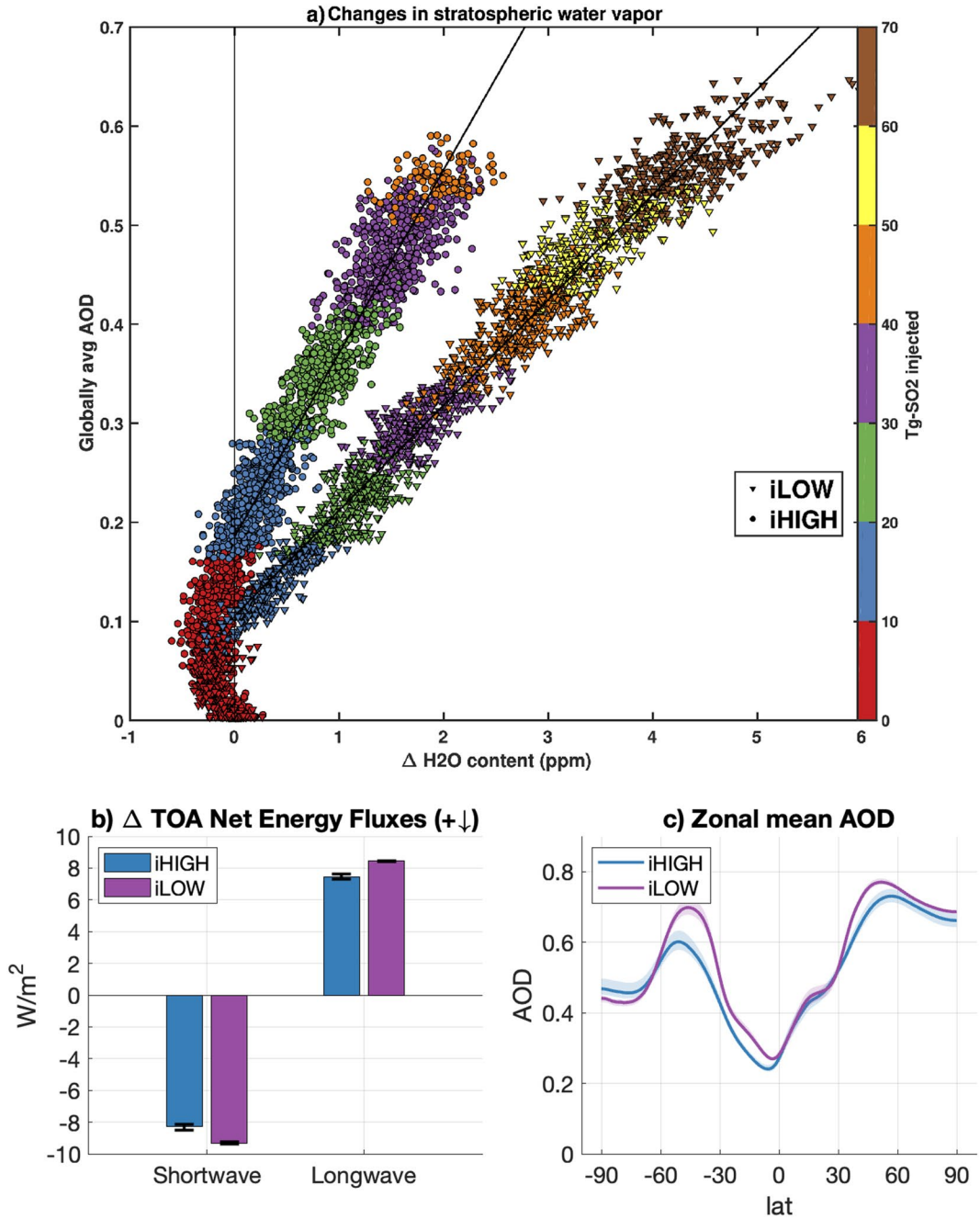


**Figure 4.** Changes to stratospheric water vapor, top-of-atmosphere (TOA) shortwave (SW) and longwave (LW) forcing, and aerosol optical depth (AOD). Panel (a) plots monthly changes to stratospheric water vapor for iHIGH (circles) and iLOW (triangles), relative to the reference period ensemble mean, against global mean AOD. Stratospheric water vapor is computed as the integral of all water vapor above the tropopause. Each data point represents one monthly mean. Color scale indicates the quantity of $SO_2$ injected that year; black lines denote lines of best fit for each simulation for data with $\Delta H_2O(v) > 0$. Panel (b) plots global mean TOA SW and LW changes for iHIGH and iLOW (2070–2089) relative to the reference period; error bars represent ensemble spread. Forcing is shown positive downward (i.e., negative for cooling and positive for warming). Panel (c) plots zonal mean stratospheric day-night 550 nm AOD for iHIGH and iLOW (2070–2089); shading denotes ensemble spread.

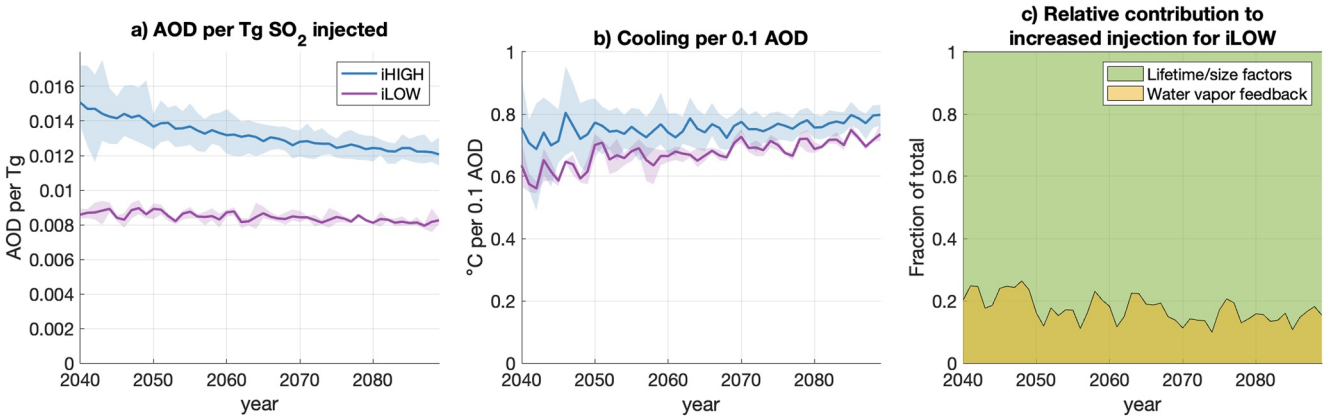


**Figure 5.** Differences in aerosol optical depth (AOD) per Tg $SO_2$ injection (a) and cooling per unit 0.1 AOD (b), which contribute to increased injection for iLOW relative to iHIGH. Shading denotes ensemble spread. Panel (c) shows the relative sizes of the increased AOD per Tg $SO_2$ injection (green) and increased cooling per 0.1 AOD (yellow) for iHIGH relative to iLOW.

causes smaller decreases in southern hemisphere column ozone than iHIGH, despite the higher injection rate (see Tilmes et al. (2021), Figure 4).

This study is also limited by the consideration of only one injection strategy and only one climate model. The relationship between injection quantity and AOD varies with injection latitude (Tilmes et al., 2017; Visioni et al., 2023; Zhang et al., 2023); therefore, the efficiency as a function of altitude, and the relative contributions of the different factors, could change for strategies which inject at latitudes other than 15° or 30°N or S, or which inject at substantially different ratios at these latitudes. Aerosol representation also remains an important source of uncertainty in climate model projections of SAI impacts, and considering similar studies across multiple models would help bound and quantify uncertainty as to how different factors and feedbacks affect SAI efficiency, and why. For instance, while we find that the longer net lifetime of high-altitude aerosols is not offset by the reduced lifetime due to coagulation (and that the net sum of these opposing effects on total injection rate is still much larger than the sum of radiative feedbacks), not all studies agree; Kleinschmitt et al. (2018), who injected at the equator using a different model, reported that these two effects were comparable enough to cancel out, with AOD per unit injection approximately constant with injection altitude. This may be due to SAI locking the quasi-biennial oscillation (QBO) into a permanent easterly shear under equatorial SAI, resulting in greater tropical confinement of aerosols (Aquila et al., 2014; Niemeier et al., 2020). Lastly, we note that while we use two broad categories—lifetime and size factors, and radiative feedbacks—based on whether they affect AOD per unit injection rate or cooling per unit AOD, respectively, other factors and feedbacks not considered here could be important in other models or in a real-world deployment scenario. For example, we neglect the methane feedback because aerosols are not coupled to the photolysis scheme in our model, but in another study with a different model the contribution of the methane feedback was found to be larger than that of the water vapor feedback (Visioni et al., 2017).

## Data Availability Statement

Computing and data storage resources, including the Cheyenne supercomputer (https://doi.org/10.5065/D6RX99HX), were provided by the Computational and Information Systems Laboratory (CISL) at NCAR. All simulations were carried out on the Cheyenne high-performance computing platform https://www2.cisl.ucar.edu/user-support/acknowledging-ncarcisl, and are available to the community via the Earth System Grid (see information at http://www.cesm.ucar.edu/projects/community-projects/GLENS/).

**Acknowledgments**
We would like to acknowledge high-performance computing support from Cheyenne (https://doi.org/10.5065/D6RX99HX) provided by NCAR's Computational and Information Systems Laboratory, sponsored by the National Science Foundation. Support for WL and DM was provided by the National Science Foundation through agreement CBET-2038246. Support for DV and EMB was provided by the Atkinson Center for a Sustainable Future at Cornell University. Support for EMB was also provided by the NOAA cooperative agreement NA22OAR4320151 and the NOAA Earth's Radiative Budget initiative. Support for BK was provided in part by the National Sciences Foundation through agreement SES-1754740 and the Indiana University Environmental Resilience Institute. The Pacific Northwest National Laboratory is operated for the U.S. Department of Energy by Battelle Memorial Institute under contract DE-AC05-76RL01830. The CESM project is supported primarily by the National Science Foundation. This work was supported by the National Center for Atmospheric Research, which is a major facility sponsored by the National Science Foundation under Cooperative Agreement No. 1852977.

## References

Aquila, V., Garfinkel, C. I., Newman, P., Oman, L., & Waugh, D. (2014). Modifications of the quasi-biennial oscillation by a geoengineering perturbation of the stratospheric aerosol layer. *Geophysical Research Letters*, *41*(5), 1738–1744. https://doi.org/10.1002/2013GL058818

Bednarz, E. M., Butler, A. H., Visioni, D., Zhang, Y., Kravitz, B., & MacMartin, D. G. (2023). Injection strategy—A driver of atmospheric circulation and ozone response to stratospheric aerosol geoengineering. *EGUsphere*, 1–32. https://doi.org/10.5194/egusphere-2023-495

Bednarz, E. M., Visioni, D., Kravitz, B., Jones, A., Haywood, J. M., Richter, J., et al. (2023). Climate response to off-equatorial stratospheric sulfur injections in three Earth System Models—Part 2: Stratospheric and free-tropospheric response. *Atmospheric Chemistry and Physics*, *23*(1), 687–709. https://doi.org/10.5194/acp-23-687-2023

Bingaman, D. C., Rice, C. V., Smith, W., & Vogel, P. (2020). A stratospheric aerosol injection lofter aircraft concept: Brimstone angel. In *AIAA Scitech 2020 Forum*. https://doi.org/10.2514/6.2020-0618

Dykema, J. A., Keith, D. W., & Keutsch, F. N. (2016). Improved aerosol radiative properties as a foundation for solar geoengineering risk assessment. *Geophysical Research Letters*, *43*(14), 7758–7766. https://doi.org/10.1002/2016GL069258

Heckendorn, P., Weisenstein, D., Fueglistaler, S., Luo, B. P., Rozanov, E., Schraner, M., et al. (2009). The impact of geoengineering aerosols on stratospheric temperature and ozone. *Environmental Research Letters*, *4*(4), 045108. https://doi.org/10.1088/1748-9326/4/4/045108

Hurrell, J. W., Holland, M. M., Gent, P. R., Ghan, S., Kay, J. E., Kushner, P. J., et al. (2013). The community Earth system model: A framework for collaborative research. *Bulletin of the American Meteorological Society*, *94*(9), 1339–1360. https://doi.org/10.1175/BAMS-D-12-00121.1

Kleinschmitt, C., Boucher, O., & Platt, U. (2018). Sensitivity of the radiative forcing by stratospheric sulfur geoengineering to the amount and strategy of the $SO_2$ injection studied with the LMDZ-S3A model. *Atmospheric Chemistry and Physics*, *18*(4), 2769–2786. https://doi.org/10.5194/acp-18-2769-2018

Kravitz, B., MacMartin, D. G., Mills, M. J., Richter, J. H., Tilmes, S., Lamarque, J.-F., et al. (2017). First simulations of designing stratospheric sulfate aerosol geoengineering to meet multiple simultaneous climate objectives. *Journal of Geophysical Research: Atmospheres*, *122*(23), 12616–12634. https://doi.org/10.1002/2017JD026874

Krishnamohan, K., Bala, G., Cao, L., Duan, L., & Caldeira, K. (2020). The climatic effects of hygroscopic growth of sulfate aerosols in the stratosphere. *Earth's Future*, *8*(2), e2019EF001326. https://doi.org/10.1029/2019EF001326

Krishnamohan, K.-P. S.-P., Bala, G., Cao, L., Duan, L., & Caldeira, K. (2019). Climate system response to stratospheric sulfate aerosols: Sensitivity to altitude of aerosol layer. *Earth System Dynamics*, *10*(4), 885–900. https://doi.org/10.5194/esd-10-885-2019

Lee, W., MacMartin, D., Visioni, D., & Kravitz, B. (2020). Expanding the design space of stratospheric aerosol geoengineering to include precipitation-based objectives and explore trade-offs. *Earth System Dynamics*, *11*(4), 1051–1072. https://doi.org/10.5194/esd-11-1051-2020

Liu, X., Easter, R. C., Ghan, S. J., Zaveri, R., Rasch, P., Shi, X., et al. (2012). Toward a minimal representation of aerosols in climate models: Description and evaluation in the Community Atmosphere Model CAM5. *Geoscientific Model Development*, *5*(3), 709–739. https://doi.org/10.5194/gmd-5-709-2012

MacMartin, D. G., Kravitz, B., Tilmes, S., Richter, J. H., Mills, M. J., Lamarque, J.-F., et al. (2017). The climate response to stratospheric aerosol geoengineering can be tailored using multiple injection locations. *Journal of Geophysical Research: Atmospheres*, *122*(23), 12574–12590. https://doi.org/10.1002/2017JD026868

MacMartin, D. G., Visioni, D., Kravitz, B., Richter, J. H., Felgenhauer, T., Lee, W. R., et al. (2022). Scenarios for modeling solar radiation modification. *Proceedings of the National Academy of Sciences of the United States of America*, *119*(33). https://doi.org/10.1073/pnas.2202230119

McClellan, J., Keith, D. W., & Apt, J. (2012). Cost analysis of stratospheric albedo modification delivery systems. *Environmental Research Letters*, *7*(3), 034019. https://doi.org/10.1088/1748-9326/7/3/034019

Meinshausen, M., Smith, S. J., Calvin, K., Daniel, J. S., Kainuma, M. L. T., Lamarque, J.-F., et al. (2011). The RCP greenhouse gas concentrations and their extensions from 1765 to 2300. *Climatic Change*, *109*(213), 213–241. https://doi.org/10.1007/s10584-011-0156-z

Mills, M. J., Richter, J. H., Tilmes, S., Kravitz, B., MacMartin, D. G., Glanville, A. A., et al. (2017). Radiative and chemical response to interactive stratospheric sulfate aerosols in fully coupled CESM1(WACCM). *Journal of Geophysical Research: Atmospheres*, *122*(23), 13061–13078. https://doi.org/10.1002/2017JD027006

National Academies of Sciences, Engineering, and Medicine. (2021). *Reflecting sunlight: Recommendations for solar geoengineering research and research governance*. The National Academies Press. https://doi.org/10.17226/25762

Niemeier, U., Richter, J. H., & Tilmes, S. (2020). Differing responses of the quasi-biennial oscillation to artificial $SO_2$ injections in two global models. *Atmospheric Chemistry and Physics*, *20*(14), 8975–8987. https://doi.org/10.5194/acp-20-8975-2020

Niemeier, U., Schmidt, H., & Timmreck, C. (2011). The dependency of geoengineered sulfate aerosol on the emission strategy. *Atmospheric Science Letters*, *12*(2), 189–194. https://doi.org/10.1002/asl.304

Niemeier, U., & Timmreck, C. (2015). What is the limit of climate engineering by stratospheric injection of $SO_2$? *Atmospheric Chemistry and Physics*, *15*(16), 9129–9141. https://doi.org/10.5194/acp-15-9129-2015

Pierce, J. R., Weisenstein, D. K., Heckendorn, P., Peter, T., & Keith, D. W. (2010). Efficient formation of stratospheric aerosol for climate engineering by emission of condensible vapor from aircraft. *Geophysical Research Letters*, *37*(18). https://doi.org/10.1029/2010GL043975

Quaglia, I., Visioni, D., Pitari, G., & Kravitz, B. (2022). An approach to sulfate geoengineering with surface emissions of carbonyl sulfide. *Atmospheric Chemistry and Physics*, *22*(9), 5757–5773. https://doi.org/10.5194/acp-22-5757-2022

Richter, J., Visioni, D., MacMartin, D., Bailey, D., Rosenbloom, N., Lee, W., et al. (2022). Assessing responses and impacts of solar climate intervention on the Earth system with stratospheric aerosol injection (ARISE-SAI). *EGUsphere*, 1–35. https://doi.org/10.5194/egusphere-2022-125

Smith, W., Bhattarai, U., Bingaman, D. C., Mace, J. L., & Rice, C. V. (2022). Review of possible very high-altitude platforms for stratospheric aerosol injection. *Environmental Research Communications*, *4*(3), 031002. https://doi.org/10.1088/2515-7620/ac4f5d

Smith, W., & Wagner, G. (2018). Stratospheric aerosol injection tactics and costs in the first 15 years of deployment. *Environmental Research Letters*, *13*(12), 124001. https://doi.org/10.1088/1748-9326/aae98d

Tilmes, S., Richter, J. H., Kravitz, B., MacMartin, D. G., Glanville, A. S., Visioni, D., et al. (2021). Sensitivity of total column ozone to stratospheric sulfur injection strategies. *Geophysical Research Letters*, *48*(19), e2021GL094058. https://doi.org/10.1029/2021GL094058

Tilmes, S., Richter, J. H., Kravitz, B., MacMartin, D. G., Mills, M. J., Simpson, I. R., et al. (2018). CESM1(WACCM) stratospheric aerosol geoengineering large ensemble project. *Bulletin of the American Meteorological Society*, *99*(11), 2361–2371. https://doi.org/10.1175/BAMS-D-17-0267.1

Tilmes, S., Richter, J. H., Mills, M. J., Kravitz, B., MacMartin, D. G., Garcia, R. R., et al. (2018). Effects of different stratospheric $SO_2$ Injection altitudes on stratospheric chemistry and dynamics. *Journal of Geophysical Research: Atmospheres*, *123*(9), 4654–4673. https://doi.org/10.1002/2017JD028146

Tilmes, S., Richter, J. H., Mills, M. J., Kravitz, B., MacMartin, D. G., Vitt, F., et al. (2017). Sensitivity of aerosol distribution and climate response to stratospheric $SO_2$ injection locations. *Journal of Geophysical Research: Atmospheres*, *122*(23), 12591–12615. https://doi.org/10.1002/2017JD026888

Visioni, D., Bednarz, E. M., Lee, W. R., Kravitz, B., Jones, A., Haywood, J. M., & MacMartin, D. G. (2023). Climate response to off-equatorial stratospheric sulfur injections in three Earth System Models—Part 1: Experimental protocols and surface changes. *Atmospheric Chemistry and Physics*, *23*(1), 663–685. https://doi.org/10.5194/acp-23-663-2023

Visioni, D., MacMartin, D. G., & Kravitz, B. (2021). Is turning down the sun a good proxy for stratospheric sulfate geoengineering? *Journal of Geophysical Research: Atmospheres*, *126*(5), e2020JD033952. https://doi.org/10.1029/2020JD033952

Visioni, D., MacMartin, D. G., Kravitz, B., Tilmes, S., Mills, M. J., Richter, J. H., & Boudreau, M. P. (2019). Seasonal injection strategies for stratospheric aerosol geoengineering. *Geophysical Research Letters*, *46*(13), 7790–7799. https://doi.org/10.1029/2019GL083680

Visioni, D., Pitari, G., & Aquila, V. (2017). Sulfate geoengineering: A review of the factors controlling the needed injection of sulfur dioxide. *Atmospheric Chemistry and Physics*, *17*(6), 3879–3889. https://doi.org/10.5194/acp-17-3879-2017

Visioni, D., Pitari, G., di Genova, G., Tilmes, S., & Cionni, I. (2018). Upper tropospheric ice sensitivity to sulfate geoengineering. *Atmospheric Chemistry and Physics*, *18*(20), 14867–14887. https://doi.org/10.5194/acp-18-14867-2018

Zhang, Y., MacMartin, D. G., Visioni, D., Bednarz, E., & Kravitz, B. (2023). Introducing a comprehensive set of stratospheric aerosol injection strategies. *EGUsphere*, 1–32. https://doi.org/10.5194/egusphere-2023-117

## References From the Supporting Information

Visioni, D., Tilmes, S., Bardeen, C., Mills, M., MacMartin, D. G., Kravitz, B., & Richter, J. H. (2022). Limitations of assuming internal mixing between different aerosol species: A case study with sulfate geoengineering simulations. *Atmospheric Chemistry and Physics*, *22*(3), 1739–1756. https://doi.org/10.5194/acp-22-1739-2022